A Comparison of Prosthetic Ear Models Created from Data Captured by Computerized Tomography, Magnetic Resonance Imaging, and Laser Scanning

Trevor J. Coward, PhD, MPhil, MIMPT[a]/Brendan J. J. Scott, BDS, BSc, PhD, FDSRCS(Ed)[b]/
Roger M. Watson, BDS, MDS, FDSRCS[c]/Robin Richards, BSc, MSc, PhD[d]

Purpose: To compare the dimensional measurements and surface topography of stereolithographic models generated from computerized tomography (CT), magnetic resonance imaging (MRI), and laser scanning (LS) data with the same subjects' natural ears and ear casts. ***Materials and Methods:*** Stereolithographic models were manufactured from images of the subjects' ears and ear casts recorded by CT, MRI, and LS, and dimensional measurements were compared. In the second part of the study, all stereolithographic models were CT scanned and reconstructed in an STL file format. A comparison of the surface topography of the CT, MRI, and LS model ears was made. ***Results:*** Intraclass correlation coefficients indicated that dimensions could be reliably measured on the CT, MRI, and LS stereolithographic models. A 2-way analysis of variance revealed no statistical differences between the various sources of data (P = .991). The smallest differences of surface topography were observed on the MRI/CT superimpositions. ***Conclusion:*** The dimensional measurements on the stereolithographic models were similar to those from the original source. Only small differences were apparent between the surface topography of the CT, MRI, and LS models. MRI may be particularly appropriate to fabricate a prosthesis because it involves no radiation for the patient and internal form can be reproduced. The use of this technique in clinical practice requires further study. *Int J Prosthodont 2007;20:275–285.*

Absence of all or part of the external ear may be acquired (eg, surgical resection or trauma) or congenital (eg, hemifacial microsomia). Rehabilitation of this defect can be achieved by either autogenous surgical reconstruction or prosthetic rehabilitation.[1,2] Whichever treatment is selected, the patient should receive guidance and advice from an expert team committed to optimal care. With congenital defects such as microtia, in which one ear is often missing, existing facial asymmetry makes it difficult to determine the size and location of either a reconstructed or prosthetic ear that will maintain facial harmony. Regardless of the treatment plan, information is needed from the existing normal contralateral ear, such as its position, level, and prominence, to plan the location and shape of the reconstructed ear or prosthesis.[3–6]

The fabrication of an artificial ear has traditionally been carried out by a maxillofacial technician, who builds a wax ear that is ultimately used to construct a mold for the final prosthesis. The production of this wax ear, which should match the normal contralateral ear in terms of size and shape, is dependent on the artistry and skill of the maxillofacial technician. In the last few years there has been a particular focus on the use of noncontact techniques involving imaging of the ear as a means of producing an appropriately shaped and located prosthesis.[7–12] More recent techniques of obtaining 3-dimensional (3D) data, used in conjunction

[a]*Lecturer, Department of Fixed and Removable Prosthodontics, Guy's King's & St. Thomas' Dental Institute, King's College London, England.*

[b]*Senior Lecturer/Honorary Consultant, Unit of Restorative Dental Care, Clinical Dental Sciences, Dundee Dental School, Dundee, Scotland.*

[c]*Professor Emeritus, Department of Fixed and Removable Prosthodontics, Guy's King's & St.Thomas' Dental Institute, King's College London, England.*

[d]*Senior Research Fellow, Department of Medical Physics and Bio-Engineering, University College London, England.*

Correspondence to: *Dr Trevor Coward, Department of Fixed and Removable Prosthodontics, King's College London Dental Institute at Guy's, King's & St. Thomas' Hospitals, Denmark Hill Campus, Bessemer Road, London SE5 9RS, England. Fax: +44 (0) 207 346 3775. E-mail: trevor.coward@kcl.ac.uk*

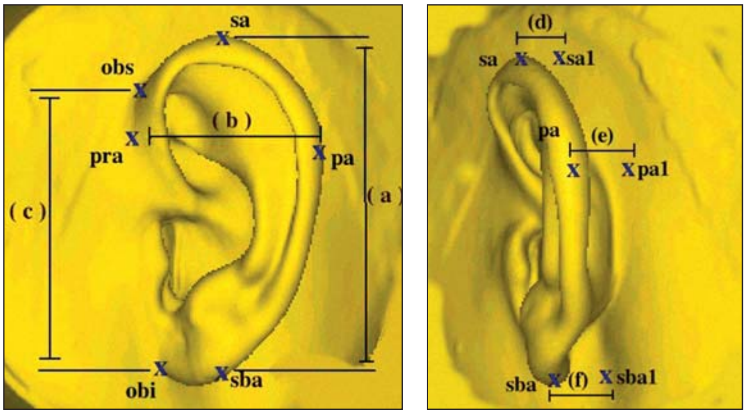

Fig 1a *(left)* Anthropometric landmarks used to record the length, width, and insertion length of the ear. X shows the individual anthropometric landmarks. Line a = sa-sba; line b = pa-pra; line c = obs-obi.

Fig 1b *(right)* Anthropometric landmarks used to record the dimensions of protrusion. X shows the individual anthropometric landmarks. Line d = sa-sa1; line e = pa-pa1; line f = sba-sba1.

with rapid prototyping techniques, allow the production of a plastic ear cast from which the wax pattern is ultimately formed.[8,11–15] This offers the potential to make a prosthesis that is more similar dimensionally to the original shape of the ear than one that has been constructed freehand. In previous studies, the use of computerized tomography (CT), magnetic resonance imaging (MRI), and laser scanning (LS) as a means of capturing 3D data was investigated.[16,17] It was generally found that the dimensions of the reconstructed ear images were similar to those from the original source,[17] which was either the natural ears or ear casts.

Although all 3 techniques have been used to the produce ear models,[6,11,14,15] no comparisons have been made regarding their accuracy. Furthermore, there has been no assessment of how these models compare dimensionally with the original source of the data (ie, the subjects' natural ears or casts made from impressions of those ears). The production of an auricular prosthesis using rapid prototyping techniques is dependent on a dimensionally accurate computer-generated image. Previous studies of CT, MRI, and LS imaging found no major differences in the dimensional measurements of the computer-generated images between each technique. Furthermore, the dimensional measurements of the images were very similar to the original sources.[16,17] This suggests that it may be possible to compare such imaging techniques in the production of an auricular prosthesis.

The main purpose of this study was to compare dimensional measurements of stereolithographic models generated from CT, MRI, and LS data with the same subjects' natural ears and ear casts. One limitation of making comparisons between dimensions alone is that it does not allow a precise assessment regarding how the overall form of the ear differs between the various sources of data. Therefore, in the second part of this study, an assessment was made of the differences in surface topography of the stereolithographic model ears derived from the 3 imaging techniques.

Materials and Methods

Sixteen patients with hemifacial microsomia were referred for rehabilitation with an implant-supported auricular prosthesis. Two of the patients were omitted from the study, as they could not fulfill the requirements of the scanning criteria. This was principally because one patient had a cardiac pacemaker and the other had ferrometallic clips in the jaw. Both conditions are contraindications for an MRI scan. Thus, the study was undertaken on 14 subjects (8 male, 6 female) with hemifacial microsomia who had normally developed facial form on one side and abnormally developed facial form on the other. All 14 subjects presented with varying degrees of hard and soft tissue deformities, which included compromised development of the mandible relative to the ascending ramus. They had an age range of 9 to 61 years (mean age: 27 years, 3 months; SD: 14 years, 2 months). All measurements and procedures were carried out on the side of the face with normal facial form and ear structure. Ethical approval was given by the Research Ethics Committee, King's Healthcare NHS Trust.

Identification of Landmarks and Dimensional Measurements

In this study, 6 standard anthropometric landmarks and 3 additional landmarks as defined by Coward[13] were used to record 6 dimensional measurements: length (sa-sba), width (pa-pra), insertion length (obs-obi), and 3 protrusive measurements (sa-sa1, pa-pa1, and sba-sba1). These landmarks are shown in Figs 1a and 1b and have been fully described previously.[17] Further, the techniques for constructing the casts and using digital calipers to record the dimensional measurements were reported in the same study.[17]

Figs 2a and 2b The 3D data files were converted into stereolithographic (STL) format **(a)**, which can be surface shaded to make the shape easier to interpret **(b)**.

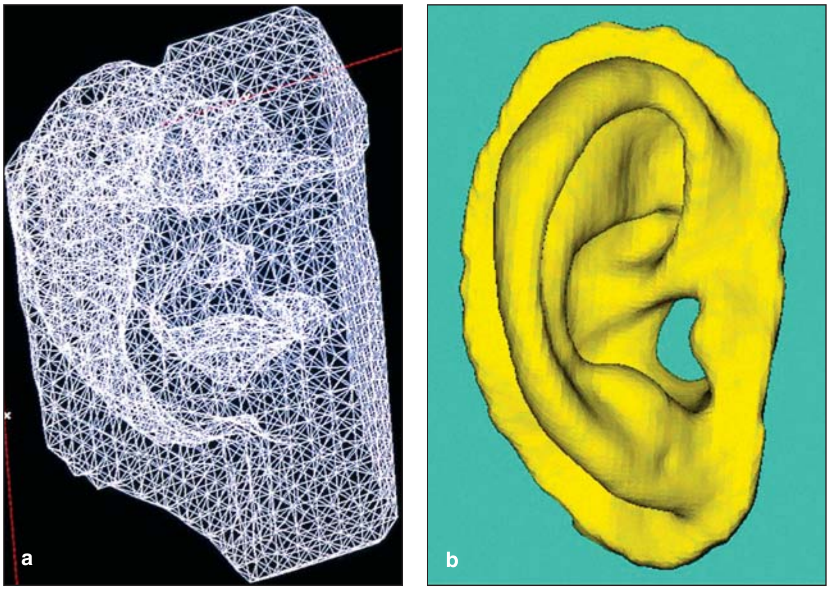

Fig 3a Model ear from CT data.

Fig 3b Model ear from MRI data.

Fig 3c Model ear from LS data.

Scanning Procedures and Production of STL Models

The original data from the CT and LS procedures described by Coward et al[17] were used in the present experiments. Because it was not possible to construct a well-defined image from an MRI scan of a plaster cast, these data were obtained from the original scans of the subjects' natural ears.[17]

The reconstructed images of each subject's ear and ear cast recorded by CT, MRI, and LS were saved as separate files. These files were converted to an STL format, which represents the surface geometry as a polygon mesh (Figs 2a and 2b). The file was sliced into a series of layers and fed as a slice file into the stereolithographic machine (SLA-250, 3D Systems 26081) to build the ear models in acrylate photopolymer (Styles Rapid Product Development) (Figs 3a to 3c).

Dimensional Measurements Recorded on the Subjects, Casts, and Stereolithographic Models

For each dimension, the mean of the 2 direct measurements recorded at intervals of no less than 1 month apart was recorded with digital calipers (Mitutoyo Measurement Technology). The 6 dimensional measurements taken from the 14 subjects' normal ears were compared to similar dimensional measurements recorded from the cast and stereolithographic models of the same ear.

Table 1 Details of Scanner and Data Acquisition for STL Models

CT scanning data
Siemens Somatom Plus 4 Scanner (Siemens Medical)
KV 120, MA 90
Matrix: 1024 mm
Field of view: 100 × 100 mm
44 to 79 slices (depending on ear size)
Slice width: 1 mm
Collimation: 1 mm
Speed of Rotation: 0.75 s
Resolution :512
AB50

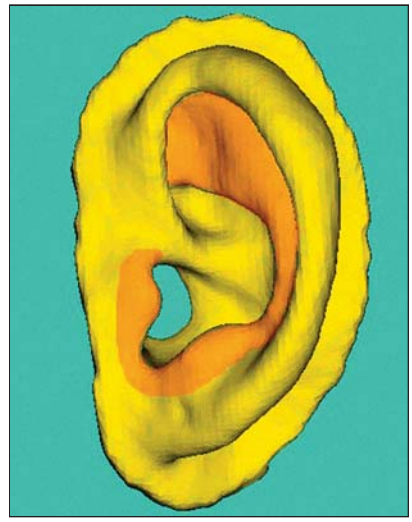

Fig 4 *(right)* STL file of CT image of the model originally produced from MRI data. The ear image is highlighted (orange) and 100 random markers are applied to orientate the CT image.

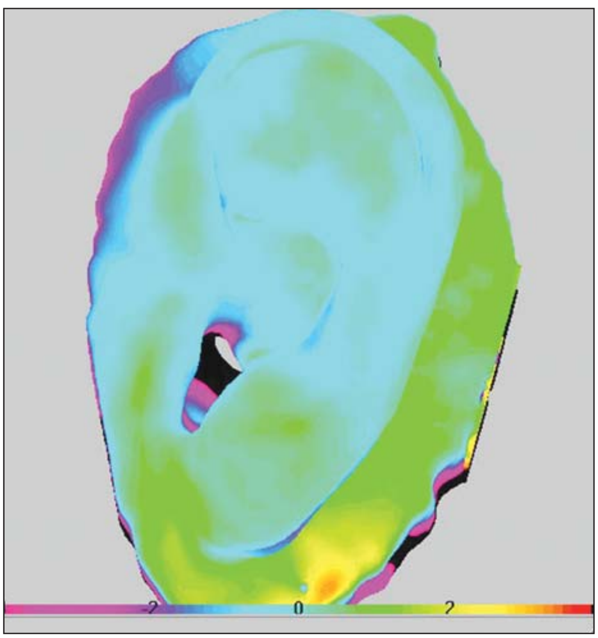

Fig 5 CT image superimposed onto an MRI image, revealing a good match of surfaces as shown by color coding (color scale is in mm). The middle of the color scale (ie, 0) represents the best match.

Surface Topography of STL Models

To study surface topography by means of superimposition of the images, it was necessary to scan each of the stereolithographic models that had been generated in the same format. CT scanning was selected as the preferred method for obtaining the data from each image source because it could reproduce all of the internal undercut surfaces on the models, which LS could not. Further, MRI was not used because it has been shown to be unpredictable.[17]

The surface topography of the stereolithographic model ears derived from the 3 methods of scanning was compared using a customized software program developed specifically for this purpose. The stereolithographic models of the 14 subjects were CT scanned and reconstructed in STL file format as 3D images. Typically, the scans of each subject's STL model were acquired using a 1-mm feed with a rotation time of 0.75 seconds and a space between slices of 1 mm. This allowed the data to be reconstructed as 1-mm slices (Table 1).

The reconstructed images from the acrylate photopolymer models produced from each technique were converted into STL format for compatibility with the customized registration software program, and superimposed as follows:

- CT of MRI stereolithographic model with CT of CT stereolithographic model
- CT of MRI stereolithographic model with CT of LS stereolithographic model
- CT of CT stereolithographic model with CT of LS stereolithographic model

The differences between the surface of the first image and the nearest point on the second image were analyzed with the computer software program using a color-coded technique. The images were first aligned with each other using 5 anthropometric landmarks (sa, sba, obs, obi, and pa). To obtain the best possible superimposition of one image on another, the program required areas of the ear to be identified which were least likely to be distorted as a result of the support of underlying cartilage (ie, tragus, antihelix) (Fig 4). The areas were selected by painting the surface of the image. The computer was programmed to select 100 random points within these areas and then look for the points that were anatomically closest to them on the surface of the other image. The images were then aligned.[18] The surfaces of the images were then viewed as a color-coded difference image (Fig 5). This process was repeated several times until the best visual match was achieved between the 2 images. Five areas of the ear (helix, scapha, lobe, tragus, and concha) were examined in detail.

Initially, the difference between the images for each of the areas was noted by visual interpretation of the colors. An objective assessment of the difference between the surfaces of the images was achieved by assigning numeric values to the differences in the separation of pixels forming the 2 images. These differences ranged from –4.00 to +4.00 mm and were recorded in increments of 0.125 mm. For example, in Fig 5 the CT image was superimposed onto an image of an MRI scan. Where the 2 surfaces of the images match, a zero value is obtained for the pixel(s). A positive difference indicates that the CT image is larger and a negative value indicates that the CT image is smaller.

A quantitative assessment of the number of pixels within each selected area (1 to 5) was performed to assess the reliability of the technique. To determine the repeatability of the assessments of pixels, each STL model ear was superimposed a total of 3 times onto images from each of the other 2 groups. For each superimposition of an individual area, the number of pixels was counted. The mean number of pixels for each of the 3 superimpositions was calculated. The difference between the number of pixels for each of the 3 superimpositions and the mean number of pixels was totaled. This was expressed as an absolute mean percentage difference (Table 2). This procedure was carried out for each of the 5 areas on the 14 subjects. The absolute mean percentage differences for all 14 subjects were averaged, and the total of the differences for the 5 areas was calculated.

To prevent pixels from being counted in more than one area, the area of interest was outlined (ie, helix, lobe) and subtracted from the overall image, and the number of pixels was counted within this chosen area (Figs 6a to 6f).

Data Analysis

The intraclass correlation coefficients were calculated to assess the reliability of the repeated measurements for each dimension. These were assessed for measurements on the CT, MRI, and LS models. Intraclass correlation coefficients for the natural ear and ear cast have been previously reported.[17] The mean of 2 measurements for each of the 6 dimensions were analyzed using a 2-way analysis of variance (ANOVA) to determine whether there were significant differences between the different sources of data (ie, direct measurements from the subjects' ears, casts of the ears, and stereolithographic models of the ears obtained from CT, MRI, and LS data). Statistical calculations were carried out with SPSS 11.5 software (SPSS).

Table 2 The Calculation of the Absolute Mean Percentage Difference for a Single Area on 1 Subject for the Superimposition of a CT and MRI Image*

	No. of pixels	Difference value
Superimposition 1	a	$d = \lvert a - g \rvert$
Superimposition 2	b	$e = \lvert b - g \rvert$
Superimposition 3	c	$f = \lvert c - g \rvert$
Mean no. of pixels	$g = (a + b + c) / 3$	
Total difference value		$h = (d + e + f)$
Absolute mean percentage difference		$m = (h / g) \times 100$

*The symbols in the difference value column indicate that the sign of the value does not form part of the calculations for the absolute mean percentage difference.

Observation of the 3 readings of the superimpositions suggested that the difference readings were so close to one another in magnitude that it would be acceptable to use the first reading alone for all subsequent analyses. The mean number of pixels for the 14 subjects was calculated for each of the 5 areas. These were used in subsequent calculations to obtain the absolute percentage differences between the 2 surface areas and were recorded for intervals of 1.00 mm, 2.00 mm, and 3.00 mm or less. The sum of the absolute percentage differences of the 5 areas between the surface topography of the reconstructed ear images was calculated (CT/MRI, CT/LS, and MRI/LS).

Results

Dimensional Measurements

There were no difficulties in the identification of landmarks on the natural ears of the 14 subjects and the casts. Similarly, landmarks were readily located on the CT and LS models of the cast and the MRI scan of the natural ear.

Repeatability

The differences between the 2 measurements for each of the 6 dimensions on the subjects and casts have already been reported.[17] The differences between the 2 measurements for each of the 6 dimensions on the STL models are displayed as mean differences and standard deviations for the 14 subjects (Fig 7). The intraclass correlation coefficients for the repeated measurements of the CT, MRI, and LS models were all calculated to be 0.99.

The coefficients of repeatability for each dimension using each measurement technique are shown in Table 3. Generally, these coefficients were of a small magnitude in relation to the overall dimension studied.

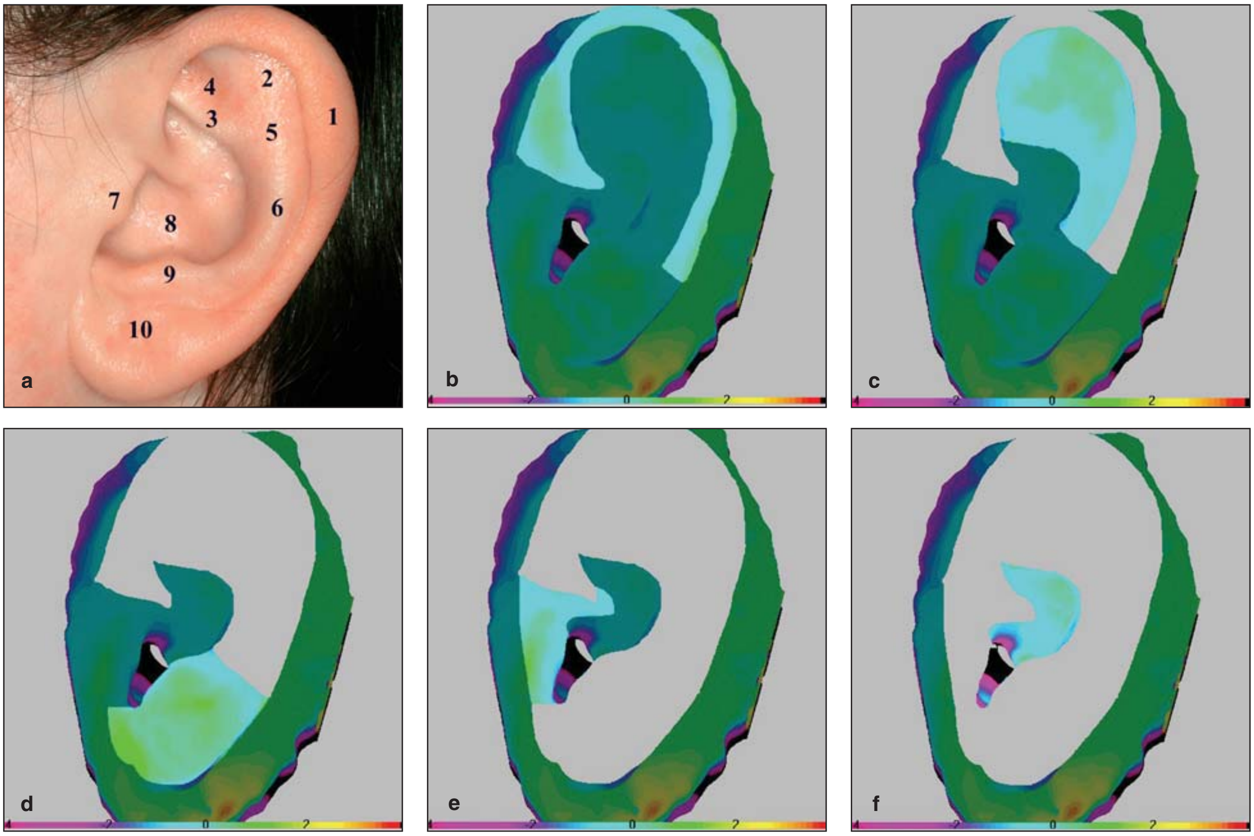

Figs 6a to 6f Sequence of assessing the number of pixels and difference between each area of the superimposed MRI/CT image. **(a)** Anatomic areas of the ear: 1 = helix; 2 = superior crus; 3 = inferior crus; 4 = fossa triangularis; 5 = scapha; 6 = antihelix; 7 = tragus; 8 = cavum conchae; 9 = antitragus; 10 = lobule. **(b)** Highlighted area 1 (helix). **(c)** Removal of area 1 and highlighted area 2 (crus, scapha, and antihelix). **(d)** Removal of area 2 and highlighted area 3 (lobe). **(e)** Removal of area 3 and highlighted area 4 (tragus). **(f)** Removal of area 4 and highlighted area 5 (concha).

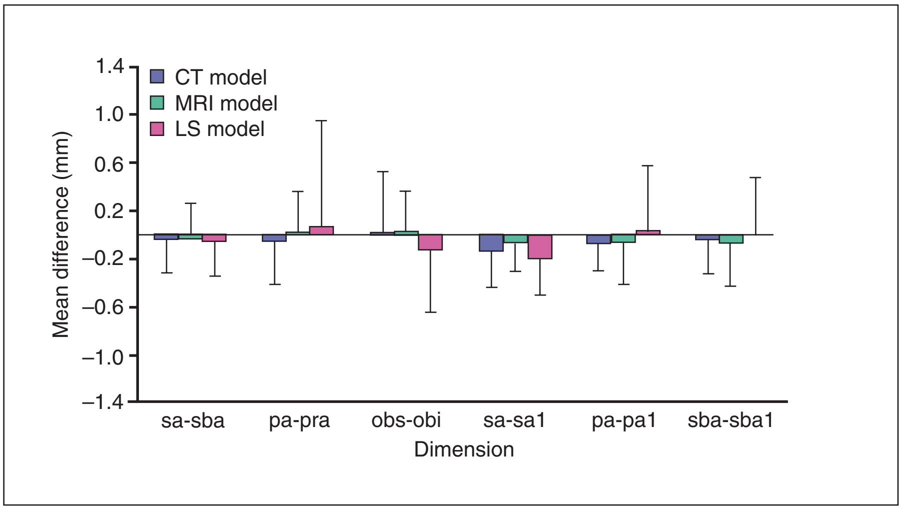

Fig 7 Differences between measurements 1 and 2 of reconstructed CT, MRI, and LS models (error bars represent standard deviations). Each individual bar represents the mean difference between the repeated readings for each dimension on the 14 subjects. The mean differences for the 2 readings are shown by red bars for the CT model, blue bars for the MRI model, and yellow bars for the LS model. The baseline represents no difference between the 2 measurements.

Dimensional Comparisons Between Natural Ears, Casts, and STL Models

The mean dimensional differences were very small between the casts and STL models compared with the natural ears. Figure 8 shows the mean differences and 95% confidence intervals for the major dimensions of the ear (length: sa-sba, width: pa-pra, and insertion length: obs-obi). Comparison of the direct method with the stereolithographic model ears (created from CT, MRI, and LS data) for the dimension of length revealed a mean difference of 0.22 to 0.58 mm. Similar differences were observed for the width (0.01 to 0.67 mm) and insertion length of the ear (0.18 to 0.26 mm). The largest difference between any of the STL models and the natural ear was for the width of the model constructed by LS, which showed a maximum mean difference of 0.67 mm. Two of the 3 dimensions on the cast (sa-sba and obs-obi) were slightly larger than the natural ear.

For all 3 protrusive measurements (sa-sa1, pa-pa1, and sa-sba1), the mean differences between the casts and STL models compared to the natural ears were also very small (Fig 9). The 3 protrusive dimensions on the casts were slightly smaller than those on the natural ears. Comparison of the direct method with the stereolithographic model ears (created from CT, MRI, and LS data) for sa-sa1 revealed a mean difference of 0.02 to 0.27 mm. Similar differences were observed for pa-pa1 (0.23 to 0.67 mm) and sba-sba1 (0.12 to 0.57 mm).

A comparison was made between all measurements for each dimension between the different methods of data collection. Two-way ANOVA revealed no statistical differences between the various sources of data ($P = .991$).

Table 3 Coefficients of Repeatability (mm) for 6 Dimensional Measurements Recorded on 14 STL Models Obtained from CT, MRI, and LS Data

Dimension	CT	MRI	LS
sa-sba	0.57	0.59	0.59
pa-pra	0.74	0.7	1.11
obs-obi	1.05	0.67	1.05
sa-a1	0.6	0.47	0.59
pa-b1	0.43	0.71	1.09
sba-c1	0.56	0.74	0.94

Surface Topography

For each area, the absolute mean percentage differences for the superimposed images were of a very small magnitude for all combinations (MRI/CT, CT/LS, and MRI/LS). For all 3 methods of superimposition, the totals of the absolute mean percentage differences between the superimposed images were 2.67% (MRI/CT), 2.80% (CT/LS), and 2.36% (MRI/LS) (Table 4). These small percentage differences between the methods of superimposition show good consistency in identifying the selected area for assessing the differences between the pixels.

Figures 10a to 10c show the difference images generated on a scale of ± 2 mm by the 3 methods of superimposition. There were no major differences between the different combinations of superimposed images.

For the 14 subjects, using the first of the superimposition measurements the absolute percentage differences were found to be between 80% and 90% from the surface of the first image and the nearest point on the surface of the second image of less than 2 mm (Table 5a) and 3 mm (Table 5b), respectively, for the 4

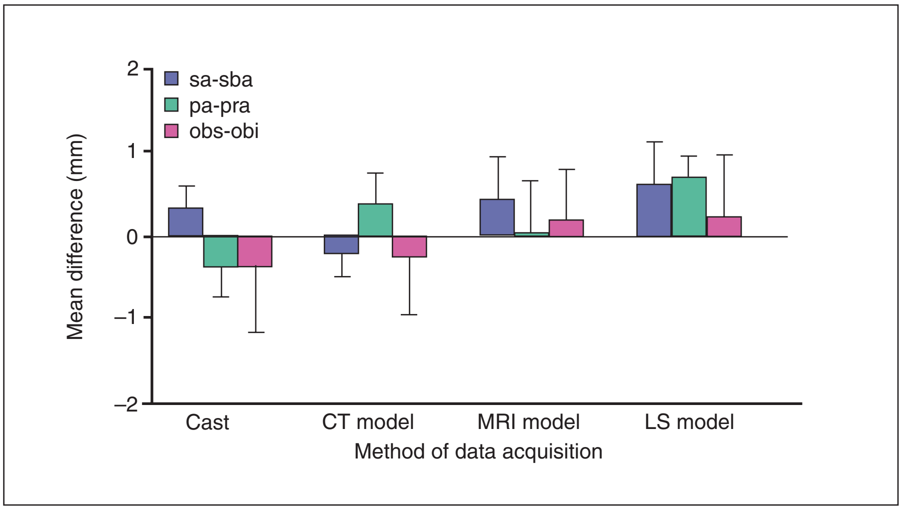

Fig 8 Mean differences between the dimensional measurements of the casts and stereolithographic models compared with the same dimensions on the natural ear (error bars represent 95% confidence intervals). A negative difference indicates the dimensional measurements were larger than the natural ear. The baseline represents no difference between the 2 measurements.

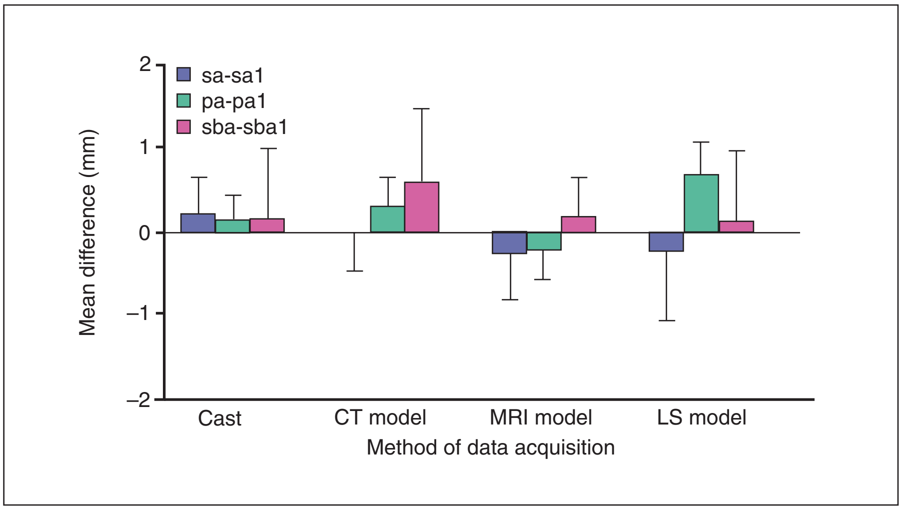

Fig 9 Mean differences between the protrusive dimensional measurements of the casts and stereolithographic models compared with the same dimensions on the natural ear (error bars represent 95% confidence intervals). A negative difference indicates the dimensional measurements were larger than the natural ear. The baseline represents no difference between the 2 measurements.

Table 4 Absolute Mean Percentage Differences (No. of Pixels) for All 5 Areas Selected from 3 Readings

Area	MRI/CT	Mean no. of pixels	CT/LS	Mean no. of pixels	MRI/LS	Mean no. of pixels
Helix	0.49 (148.51)	30,148.55	0.17 (51.42)	30,675.88	0.20 (65.53)	29,604.83
Scapha/antihelix	0.08 (19.24)	23,042.00	0.27 (66.63)	23,747.81	0.25 (60.03)	24,774.32
Lobe	0.55 (116.21)	21,221.05	0.92 (201.87)	21,654.22	0.31 (67.76)	21,939.79
Tragus	0.28 (18.13)	6,519.224	1.24 (78.80)	6,412.667	0.91 (58.07)	6,349.952
Concha	1.27 (137.79)	10,841.12	0.20 (24.16)	11,421.42	0.69 (78.42)	12,110.19
Total	2.67		2.80		2.36	

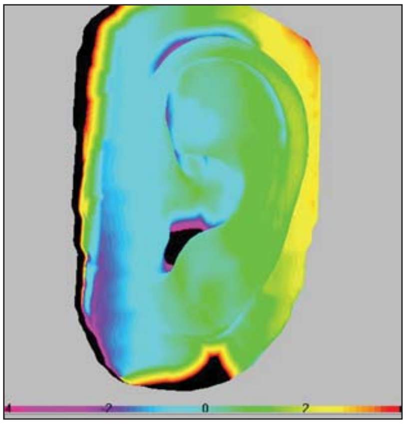

Fig 10a CT/LS superimposition.

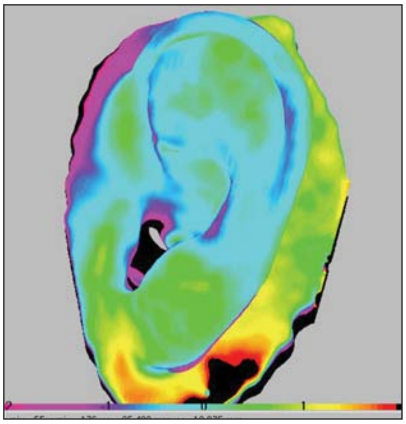

Fig 10b MRI/CT superimposition.

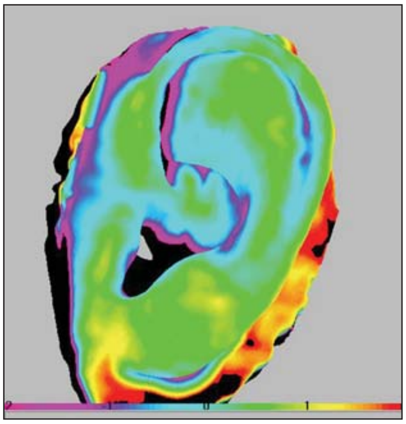

Fig 10c MRI/LS superimposition.

areas assessed (helix, scapha/antihelix, lobe, tragus). The absolute percentage difference for the fifth area (concha) in all 3 sets of images was no greater than 70% (Table 5a) and 91% (Table 5b), respectively.

For the combined areas of the ear, the absolute mean percentage differences of less than 3 mm between the images revealed that the MRI/CT superimposition showed the least difference between the topography of the 2 surfaces (ie, the most accurate superimposition). In contrast, the MRI/LS superimposition showed the greatest absolute percentage difference (ie, the least accurate superimposition). The CT/LS superimposition fell in the middle (Table 6). It was noted that for the 2 mm absolute percentage differences, CT/LS showed the least difference between the topography of the 2 surfaces.

Table 5a Absolute Mean Percentage Differences Between Individual Areas 2 mm or Less for 14 Subjects Using the First Reading

Area	CT/LS	SD	MRI/CT	SD	MRI/LS	SD
Helix	95.03	5.29	90.42	13.99	91.82	8.99
Scapha/antihelix	90.88	9.18	91.63	11.86	83.63	9.41
Lobe	97.15	3.12	87.71	15.84	80.21	25.72
Tragus	88.45	12.01	90.10	14.28	90.42	10.08
Concha	37.60	7.81	69.59	21.48	39.02	12.56

Table 5b Absolute Mean Percentage Differences Between Individual Areas 3 mm or Less for 14 Subjects Using the First Reading

Area	CT/LS	SD	MRI/CT	SD	MRI/LS	SD
Helix	98.61	3.35	98.62	4.47	98.78	1.98
Scapha/antihelix	98.51	4.47	97.53	4.67	95.32	4.93
Lobe	98.41	2.67	97.59	4.92	94.36	11.96
Tragus	92.86	10.50	98.20	3.97	96.71	5.09
Concha	61.51	15.38	90.78	12.38	66.01	16.94

Discussion

This study has shown that it is possible to create 3D models using a rapid prototyping technique with similar dimensions and surface topography from all 3 methods of obtaining digitized data. There were small differences between the techniques in relation to some dimensional measurements. The results of this study further develop the findings of a previous study in which it was shown that it is possible to capture data reliably using all imaging techniques either from a cast of the ear or directly from the scan of the natural ear itself.[17] The imaging of natural ears by MRI to obtain soft tissue contours has not been previously attempted. An MRI scanning sequence suitable for obtaining images of cartilage and synovial fluid was used to capture images of natural ears. This imaging technique was found to be comparable to digitized data obtained by CT and LS of a cast poured from an impression of a natural ear.

Although the sample size of 14 subjects may be considered modest, the statistical power was found to be greater than 90% for a significance level of $P = .05$ for all dimensions. This was based on a difference value of 2 mm, as it was judged that this amount would be clinically undetectable. Furthermore, Farkas[4] felt that differences between 3 to 4 mm would be clinically undetectable in relation to the width of an ear, which if true would give even greater power levels than found in the present study. For this reason the sample size of 14 subjects was judged to be more than sufficient to compare the methods of scanning in the production of stereolithographic models.

Visual assessment of the stereolithographic models revealed that those created from CT and MRI data produced all of the internal contours (see Figs 3a to 3c). However, the model ear manufactured from LS data only reproduced the surfaces that the laser beam could contact (ie, omitting undercut areas). The build layers from the stereolithographic process were visible on all surfaces of the models. However, the surfaces on the model from CT data were smoother with less obvious steps, whereas the model created from MRI data was slightly facetted. The surface topography of the model ears from LS data was smooth, but obvious incremental steps could be observed from the helical surface to the skull (protrusion). This was primarily a result of the laser beam being unable to contact the inferior surface because of the contour of the ear.

Table 6 Absolute Mean Percentage Differences of the 5 Ear Surfaces

Source	1 mm or less	2 mm or less	3 mm or less
MRI/LS	72.25	91.00	96.80
MRI/CT	76.73	94.73	98.97
CT/LS	90.85	95.86	97.96

Regardless of the imaging source, there were no difficulties in any of the scanning procedures, and the landmarks were readily identified on the stereolithographic models. This was confirmed by analysis of the repeated measurements. The digital calipers were accurate to a level of 0.01 μ, and the intraclass correlation coefficients for repeated measurements on the cast and natural ears were 0.99, indicating a high level of precision.[17] The data for the repeated measurements of the stereolithographic models obtained from CT, MRI, and LS images show that the mean differences for the 2 sets of readings were small for each dimension studied. Furthermore, the high values of the intraclass correlation coefficients (0.99) indicated that the dimensions could be measured reliably for all stereolithographic models. This is consistent with the results of the previous study, which assessed the differences in repeated measurements on the subject's ears, casts, and reconstructed images.[17]

It is acknowledged that there may be inherent variables associated with measurements that can be difficult to control precisely, such as caliper measurements of living tissue because of the inherent and variable fluent volume and differences in how calipers are applied to living tissue as opposed to a cast. However, previous studies have used repeated measurements to show that such variables are unlikely to have a major impact.[17]

The repeatability coefficient is based on 95% of the differences between the repeated measurements lying within 2 standard deviations of the mean difference.[19] Regardless of the data source, the repeatability coefficients for all measurements (sa-sba, pa-pra, obs-obi) related to the size of the ear were 1.11 mm or less. For all protrusive measurements (sa-sa1, pa-pa1, sba-sba1), the coefficients of repeatability were 1.09 mm or less. For all dimensions, a coefficient less than 1.11 mm represents a small proportion of the overall clinical measurement with respect to the size of each ear, and is less than reported in the previous study.[17]

There were only very small differences between the dimensions on the casts and stereolithographic models compared with the natural ears. The 3 major dimensions of the reconstructed ear image (length, width, and insertion length) obtained by digitized LS data had the greatest differences compared to the measurements on the natural ears. Nevertheless, they were still of a very small magnitude. This may reflect greater difficulties in identifying some of the anthropometric landmarks on LS models, possibly because their precise position was less clear. It may be that LS cannot recreate any internal areas that are undercut, but it is very unlikely that this would make the identification of the anthropometric landmarks on the surface of the ear more difficult. For the 3 dimensions of protrusion (sa-a1, pa-b1, and sba-c1), again only small differences were found between the direct measurements of the natural ears and those on the casts and stereolithographic models.

When comparing the means of each of the 6 dimensions measured, little difference existed between the 3 methods of producing stereolithographic model ears. Two-way ANOVA revealed no statistical differences between the direct measurements of the natural ears, casts, and CT, MRI, and LS stereolithographic models. There was no attempt made to correlate caliper measurements with computer measurement analyses. Both methods of measurements can be made over very small dimensions and it is unlikely that any variations would be clinically significant.

To establish the accuracy of the superimposition technique, each stereolithographic model ear was superimposed a total of 3 times onto images from the other 2 methods for each of the 14 subjects to provide an overall absolute mean percentage difference. A repeated measurements analysis indicated that there were only small differences between these 3 readings, and so the first reading was used in the subsequent analyses when comparing one source of data against another.

It is acknowledged that the use of CT to record the MRI and LS models may result in an uncontrolled variable compared to when the CT models themselves were scanned. However, data from the superimposition of the images suggest that this would be of a very small magnitude.

Only a small percentage error was revealed regarding the reliability of identifying the 5 selected areas revealed that for all 3 methods of superimposition. For each combination of superimpositions, there was a total absolute mean percentage difference of less than 3% in all 5 areas. This difference is considered to be of a small magnitude when compared to the total mean number of pixels. Therefore, the technique used to identify the selected area for assessing differences between pixels was considered to show good consistency.

The absolute mean percentage difference between pixels for superimposition of each image was 2 mm or less in more than 80% of areas 1 (helix), 2 (scapha/antihelix), 3 (lobe), and 4 (tragus), and 3 mm or less in 94% of the same areas. If the superimpositions were a perfect match, 100% of the areas would be at a value of 0 mm. The values of 80% at 2 mm and 94% at 3 mm suggest that the superimpositions were good and unlikely to be clinically apparent. For area 5 (concha), the mean absolute percentage difference between the superimposition of CT/LS and MRI/LS was 2 mm or less in 40% of the areas and 3 mm or less in 67% of the areas. For the MRI/CT superimposition, the difference was 2 mm or less in 70% of the areas and 3 mm or less in 80% of the areas. One explanation for these observations is that in the LS method, this site is more difficult to define because much of the area is undercut and in the floor of the ear. Therefore, LS is less likely to identify the full area since the projected laser line will only pick up the surfaces in view. However, the superimposition of images from CT, MRI, and LS is generally dependent on the outline form. The fact that the LS could not show internal form would not have impacted most areas in a clinically significant way.

The absolute mean percentage differences in the surface topography of all stereolithographic models revealed that a high percentage of pixels between the images were less than 3 mm apart (Table 6). The highest percentage of pixels observed for 3 mm was between the CT and MRI stereolithographic models. This would suggest that the CT and MRI models were of fairly similar topography, allowing for subject variability. It should also be noted that the original data of the MRI scan were recorded directly from the subjects' normal ears. In contrast, some of the differences between pixels from MRI/LS and MRI/CT superimpositions could reflect the fact that the CT and LS data were recorded from a stone cast of a natural ear. This would require further study.

At this stage, it would be difficult to draw conclusions about the cost efficiency of the rapid prototyping techniques versus the conventional sculpting techniques to produce prosthetic ears. One advantage of these techniques is that the technician is not required to construct the model, although they may be required to refine it. This reduction in fabrication time would have to be measured against the cost of purchasing and maintaining the imaging and sculpting devices. This would require further evaluation.

Conclusion

The results show that the 3 methods of imaging generally resulted in dimensional measurements on the stereolithographic models similar to those from the subjects' natural ears. Furthermore, very little differences were apparent between the surface topography of the images generated from the CT, MRI, and LS stereolithographic models. Although there were some differences in the models produced using LS, it is unlikely that these differences would have any clinical implications. However, there are limitations regarding internal form for the LS technique because of its inability to identify surfaces that are not directly in view. For this reason, it would seem that CT and MRI would supercede LS in a hierarchic order of choice for the production of stereolithographic model ears. Although it has been suggested that CT scanning is the most reliable[20,21] and provides the best resolution, the present study has shown that stereolithographic model ears can be created effectively from MRI scanning, which involves no radiation for the patient. The use of this technique in clinical practice requires further study.

Acknowledgments

The authors acknowledge the generous use of facilities in the Department of Bio-Engineering and Medical Physics, University College, London, and the MRI and CT units at Kings College Hospital. Particular thanks are extended to Dr Alf Linney (University College London) and Mrs Janice Mackie, Mr John Totman, and Mr Simon Gover (Kings College Hospital). We would also like to thank Dr Derek Cooper, Statistician, Information Technology Department, King's College London, for his advice.

References

1. Fine L, Robinson J, Barnhart G. Absence or major loss of part of the external ear and its correction. J Prosthet Dent 1974;31:313–322.
2. Wilkes GH, Wolfaardt JF. Osseointegrated alloplastic versus autogenous ear reconstruction: Criteria for treatment selection. Plast Reconstr Surg 1994;93:967–979.
3. Figalova P, Farkas LG. Localization of the auricle by means of anthropometric methods. Acta Chir Plast 1968;10:7–14.
4. Farkas LG. Anthropometry of normal and anomalous ears. Clin Plast Surg 1978;5:401–412.
5. Tolleth H. A hierarchy of values in the design and construction of the ear. Clin Plast Surg 1990;17:193–207.
6. Watson RM, Coward TJ, Forman GH, Moss JP. Considerations in treatment planning for implant supported prostheses. Int J Oral Maxillofac Implants 1993;8:445–449.
7. Coward TJ, Watson RM, Scott BJJ. Laser scanning for the identification of repeatable landmarks of the ears and face. Br J Plast Surg 1997;50:308–314.
8. Chen LH, Tsutsumi S, Lizuka T. A CAD/CAM technique for fabricating facial prostheses: A preliminary report. Int J Prosthodont 1997;10:467–472.
9. Coward TJ, Scott BJJ, Watson RM, Richards R. Laser scanning of the ear identifying the shape and position in subjects with normal facial symmetry. Int J Oral Maxillofac Surg 2000;29:18–23.
10. Coward TJ, Scott BJJ, Watson RM, Richards R. Identifying the position of an ear from a laser scan: The significance for planning rehabilitation. Int J Oral Maxillofac Surg 2002;31:244–251.
11. Jiao T, Zhang F, Huang X, Wang C. Design and fabrication of auricular prostheses by CAD/CAM system. Int J Prosthodont 2004;17:460–463.
12. Sykes LM, Parrot AM, Owen CP, Snaddon DR. Applications of rapid protyping in maxillofacial prostheses. Int J Prosthodont 2004;17:454–459.
13. Coward TJ. Production of Artificial Ears: Aspects of the Technical Problem [MPhil thesis]. London: University of London, 1996.
14. Coward TJ, Watson RM. Use of laser scanning systems in the fabrication of auricular prostheses. Quintessence Dent Technol 1997;20:47–54.
15. Coward TJ, Watson RM, Wilkinson IC. Fabrication of a wax ear by rapid-process modeling using stereolithography. Int J Prosthodont 1999;12:20–27.
16. Coward TJ, Scott BJJ, Watson RM, Richards R. A comparison between computerized tomography, magnetic resonance imaging, and laser scanning for capturing three dimensional data from an object of standard form. Int J Prosthodont 2005;18:405–413.
17. Coward TJ, Scott BJJ, Watson RM, Richards R. A comparison between computerized tomography, magnetic resonance imaging, and laser scanning for capturing 3-dimensional data from a natural ear to aid rehabilitation. Int J Prosthodont 2006;19:463–471.
18. Press WH, Flannery BP, Teukolsky SA, Verterling WT. Numerical recipes: The art of scientific computing. Cambridge: Cambridge University Press, 1986:509–520.
19. Bland JM, Altman DG. Statistical methods for assessing agreement between two methods of clinical measurement. Lancet 1986; 1(8476):307–310.
20. Smith DK, Berquist TH, An KN, Robb RA, Chao E. Validation of three dimensional reconstructions of knee anatomy: CT v MR imaging. J Comput Assist Tomog 1989;13:294–301.
21. Waitzman AA, Posnick JC, Armstrong DC, Pron GE. Craniofacial skeletal measurements based on computed tomography: Part 1. Accuracy and reproducibility. Cleft Palate Craniofac J 1992; 29:112–117.